SCANNING VOL. 30, 299–309 (2008)
© Wiley Periodicals, Inc.

Mapping the Electrical Properties of Semiconductor Junctions—the Electron Holographic Approach

ALISON C. TWITCHETT-HARRISON[1], RAFAL E. DUNIN-BORKOWSKI[2] and PAUL A. MIDGLEY[3]

[1]Department of Materials, Imperial College London, London, United Kingdom
[2]Center for Electron Nanoscopy, Technical University of Denmark, Kongens Lyngby, Denmark
[3]Department of Materials Science and Metallurgy, University of Cambridge, Cambridge, United Kingdom

Summary: The need to determine the electrical properties of semiconductor junctions with high spatial resolution is as pressing now as ever. One technique that offers the possibility of quantitative high-resolution mapping of two- and three-dimensional electrostatic potential distributions is off-axis electron holography. In this study, we review some of the issues associated with interpreting phase shifts measured using off-axis electron holography, and we describe how a quantitative determination of the dopant-related electrostatic potential can be achieved for device structures. Issues that include the presence of surface "dead" layers, external electrostatic fringing fields, variations in specimen thickness and dynamical diffraction are discussed, and their impact on the quantification of results obtained using off-axis electron holography is examined. SCANNING 30: 299–309, 2008. © 2008 Wiley Periodicals, Inc.

Key words: three-dimensional reconstruction, tomography, holography, metrology

Introduction

A key issue that remains paramount for the development of semiconductor device structures is the requirement to map dopant distributions in two and three dimensions quantitatively with high spatial resolution (International Technology Roadmap for Semiconductors, 2007; http://www.itrs.net/). Over the years, many characterization techniques, including secondary ion mass spectrometry (Tsukamoto *et al.* 2003), scanning probe microscopies (McMurray *et al.* 1997) and more recently atom probe tomography (Thompson *et al.* 2007), have been developed for the study of two- and three-dimensional dopant distributions. However, in general these techniques do not distinguish easily between the electrically *active* and *inactive* dopant species that are present. With shrinking device dimensions, higher concentrations of dopant atoms are implanted. However, dopant clustering can then reduce the electrically active dopant concentration. It is therefore of increasing importance to be able to map the electrically active dopant concentration quantitatively with high spatial resolution, rather than to infer it from measured or expected compositional profiles.

Scanning electron microscopy (SEM)-based electron beam-induced current (EBIC) techniques, which David Holt and co-workers pioneered for many years (e.g., Holt and Yacobi 2007 and references therein), can be used to reveal electrical properties at junctions and boundaries. EBIC and related methods have been adopted by semiconductor industries to indicate the extents of depletion regions and to investigate failure sites. As an example, Figure 1 shows a false color image of a GaAs-based avalanche photodiode device. The bright horizontal stripe indicates the high intensity of the EBIC signal that is superimposed onto a secondary electron image to indicate the spatial extent of beam-induced carriers within the intrinsic region of a p–i–n junction. Similar images can be recorded to reveal the positions of p–n junctions. More recently, low-voltage secondary electron signals have been used to reveal image contrast resulting directly from the presence of doped layers (Perovic *et al.* 1995). There is still some discussion as

Contract grant sponsor: European Union.

Address for reprints: Paul A. Midgley, Department of Materials Science and Metallurgy, University of Cambridge, Pembroke Street, Cambridge CB2 3QZ, UK, E-mail: pam33@cam.ac.uk

Received 23 May 2008; Accepted with revision 5 June 2008

DOI 10.1002/sca.20125
Published online 18 July 2008 in Wiley InterScience (www.interscience.wiley.com)

to the nature of the mechanism that generates this contrast, but it is known to be highly surface sensitive and difficult to quantify.

Although EBIC provides a very convenient method to map the positions of electrically active junctions in the SEM, it is not straightforward to reveal the underlying electrostatic potential directly and to quantify potential gradients and thus dopant concentrations. In addition, in some cases the spatial resolution offered by EBIC may not be sufficient to map the high-concentration layers that are used in many modern devices. In principle, transmission electron microscopy (TEM) techniques offer higher spatial resolution and direct sensitivity to changes in electrostatic potential. One method that can be used to reveal the positions and spatial extents of p–n junction depletion layers is Foucault imaging. This technique is traditionally used for imaging magnetic domain walls, and involves the use of the edge of an objective aperture to block part of the electron beam in the back focal plane of the objective lens. In a semiconductor device, a gradient in potential across the field of view will result in a small but usable deflection of the electron beam, analogous to the Lorentz force deflection in magnetic imaging. Figure 2 shows a pair of Foucault images indicating the presence of the depletion region at the position of a p–n junction in a simple Si device. Figure 2(a) (the dark-field (DF) image) is formed by allowing only the deflected part of the beam through the aperture. The depletion region, in which the potential is varying, then appears bright. Figure 2(b) (the bright-field image) is formed using just the nondeflected part, and the depletion region then appears dark. The two images are complementary, and the DF image is qualitatively similar in appearance to EBIC images of junctions such as that shown in Figure 1. The intensity near the depletion region in a DF Foucault image is approximately proportional to the first derivative of the projected potential, i.e. to the electric field, if the specimen thickness is uniform.

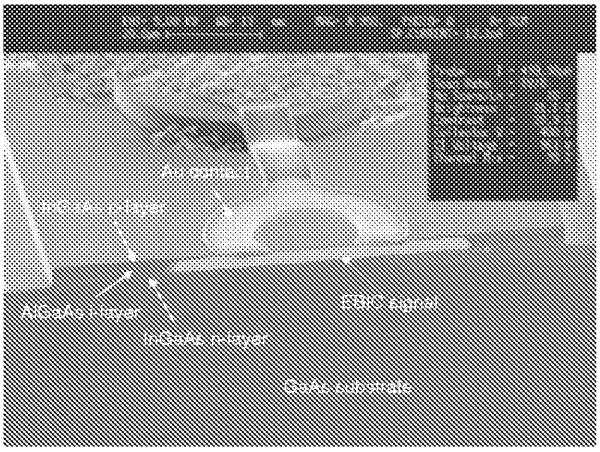

Fig 1. False color image superimposing an EBIC image and a secondary electron image of an avalanche photodiode. The intrinsic layer of the p–i–n junction is shown bright. (Image courtesy of Dr. Richard Beanland.) [The color version of this figure can be seen online at www.interscience.wiley.com/sca.]

Modern TEMs and scanning transmission electron microscopes (STEMs) are increasingly equipped with coherent sources of electrons (field emission or Schottky guns), offering the possibility of recording images based on interferometric techniques that encode phase information about the specimen in the form of interferograms (or holograms). Gabor's (1949, 1951) original idea was based on what is now called in-line electron holography, or Fresnel defocus imaging, whereby two halves of a wave interfere to produce encoded information, but where both halves have been perturbed by the specimen potential. A modern example of the formation of such an image is shown

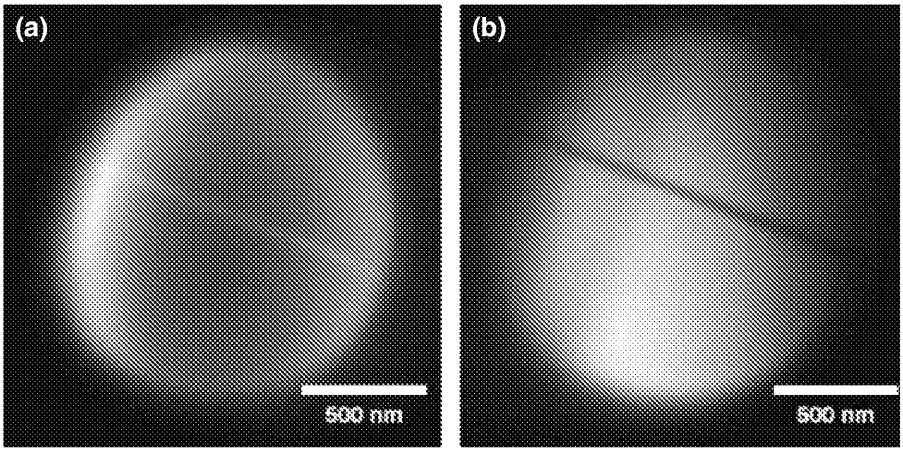

Fig 2. (a) Dark-field and (b) bright-field Foucault images of an Si p–n junction of 550-nm-thick FIB-prepared specimen obtained by using the objective aperture to select (a) the streak from the p–n junction, with the unscattered beam masked out, and (b) the unscattered beam, with the streak from the p–n junction masked out.

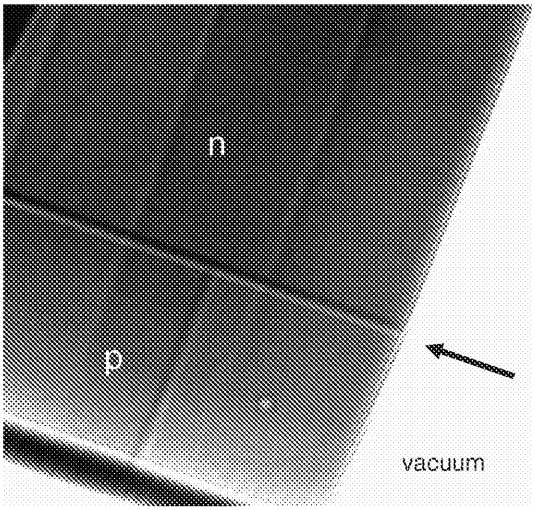

Fig 3. In-line electron hologram (Fresnel defocus image) of an FIB-prepared Si p–n junction. Black–white contrast is evident at the position of the junction (arrowed). Similar contrast running perpendicular to the junction can be seen at regions where there is a steep change in specimen thickness.

in Figure 3, which illustrates the ability to visualize the position of a p–n junction using this type of electron holography. In a similar fashion to the interpretation of the contrast seen in Figure 2, the image intensity in the defocused image at the position of the junction (arrowed) is approximately proportional to the second derivative of the potential, i.e. to the variation in charge density in the depletion region. Although practised primarily in the TEM, techniques based on Foucault and Fresnel imaging can also be implemented in the STEM, resulting in similar image contrast, although the practical setup may be different (Cowley 1992).

A third TEM technique, off-axis electron holography, allows the electrostatic potential distribution in a semiconductor device, projected in the electron beam direction, to be measured directly and quantitatively. Off-axis electron holography is also a form of interferometry, which can be used to record the phase shift of an electron wave that has passed through a specimen relative to a reference (often vacuum) wave (Midgley 2001). The phase shift is sensitive to the electro-magnetic potential within and around the specimen (projected in the incident electron beam direction) according to the equation

$$\phi(x,y) = C_E \int_L V(x,y,z)\,dz - \frac{2\pi e}{h} \times \int_L A_Z(x,y,z)\,dz \qquad (1)$$

where C_E is a microscope-determined constant, $V(x, y, z)$ is the electrostatic potential, A_Z is the component of the magnetic vector potential in the electron beam direction z and L denotes the path of the electron beam. In this study, we consider specimens in which no magnetic fields are present, and for which only electrostatic potentials play a role. For these specimens, the second term on the right-hand side of Equation (1) is zero.

Figure 4(a) shows a schematic diagram illustrating the formation of an off-axis electron hologram in the TEM. A positively charged electron biprism (usually an Au-coated quartz wire) is used to interfere part of the electron wave that has passed through the specimen with part of the electron wave that has (ideally) passed outside the specimen through a region of vacuum. The resulting interference pattern, or "hologram," contains local perturbations of the interference fringe spacing and amplitude that can be extracted numerically to reveal variations in the phase shift and amplitude of the electron wave that has passed through the specimen. Figure 4(b) shows a schematic illustration of the computational reconstruction process that is typically used to extract phase and amplitude information from experimental off-axis electron holograms. The local charge density and the electric field in the specimen can in principle be calculated from the reconstructed projected electrostatic potential distribution using Poisson's equation, if the specimen is uniform in thickness and if the specimen thickness is known. The accuracy and the precision of the quantification of the charge density rely on the spatial and phase resolutions of the reconstructed two-dimensional phase image, which are interdependent. The phase resolution, $\delta\phi$, is given by the equation

$$\delta\phi = \frac{1}{\mu}\sqrt{\frac{2}{N_t}} \qquad (2)$$

where μ is the fringe contrast and N_t is the total electron count in the effective pixel size (Lichte 1993). The spatial resolution in the reconstructed phase image is determined in part by the size of the mask that is applied to the sideband during data processing. In general, for a complex object, the maximum radius of this mask in the Fourier transform of the hologram is one-third of the distance from the center of the sideband to the origin of Fourier space (Ishizuka 1993); i.e. the maximum spatial frequency in the reconstructed phase image is one-third of the carrier frequency in the electron hologram. The interference fringe spacing, which determines the position of the sideband in the Fourier transform of the hologram, is determined by the electron-optical setup and by the magnitude of the electrostatic potential applied to the biprism wire. The higher the potential applied to the

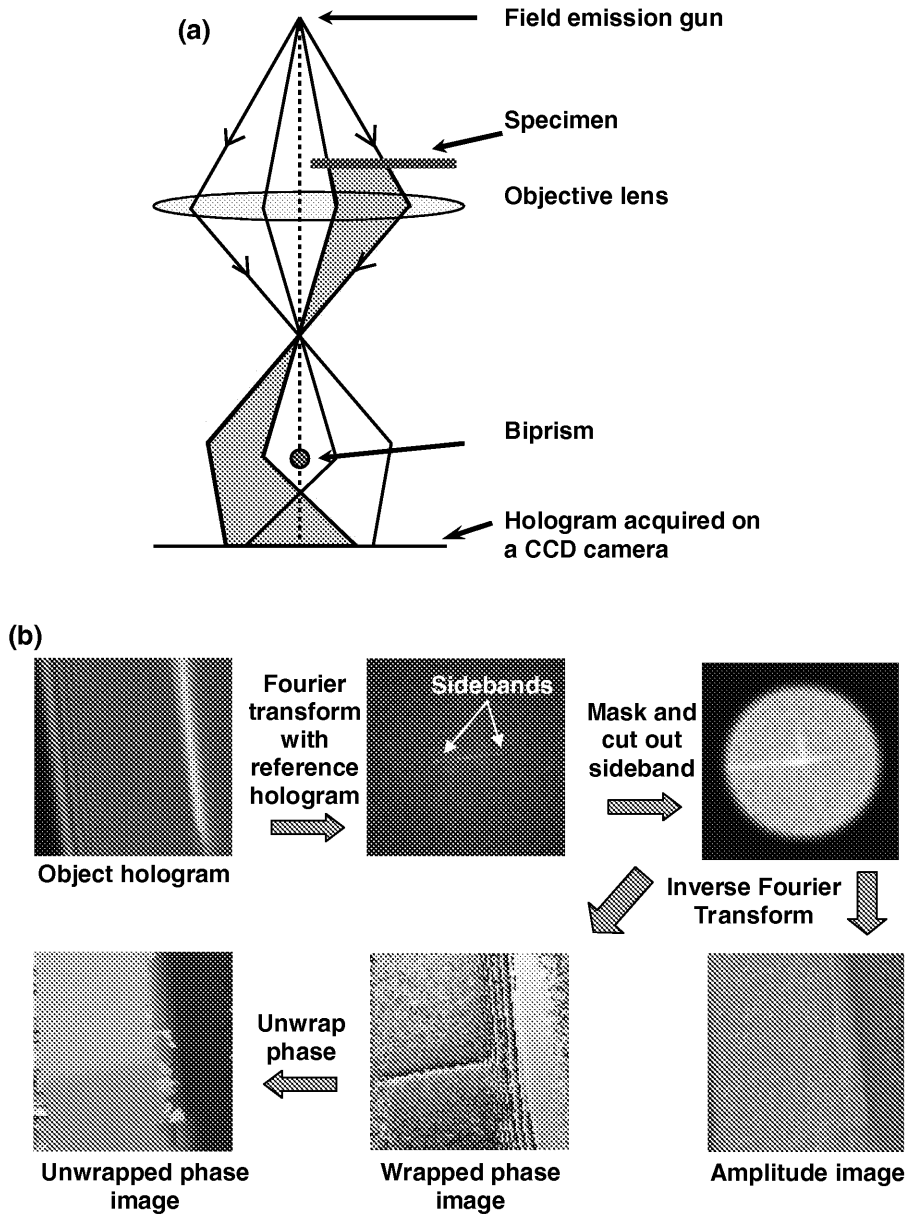

Fig 4. (a) Schematic diagram illustrating the formation of a medium resolution off-axis electron hologram in the TEM. (b) Schematic illustration of the process used to reconstruct phase and amplitude images from off-axis electron holograms. The use of a vacuum (empty) hologram is not described for clarity. [The color version of this figure can be seen online at www.interscience.wiley.com/sca.]

biprism, the finer will be the interference fringes and the better the spatial resolution. However, the interference fringe contrast is then reduced, and hence the phase resolution will be degraded. A balance between these two requirements has to be met to find the optimal hologram acquisition conditions.

According to Equation (1), the recorded phase shift at position (x, y) is related to a line projection of the electrostatic potential taking into consideration the potentials above, within and below the specimen. For a semiconductor specimen, both external electrostatic fringing fields and internal potential variations must be taken into account to be able to interpret the observed phase shift quantitatively. The interpretation can be simplified if the external electrostatic fringing fields are absent; for example, if the specimen surfaces are coated with a conductive layer of carbon to provide an equipotential specimen surface (McCartney *et al.* 2002) or if focused ion beam (FIB) specimen preparation is used (Twitchett *et al.* 2002). This possibility is discussed below. If no electrostatic fringing fields are present, then the phase shift measured experimentally is given by the equation

$$\phi = C_E \int_0^t V(x, y, z)\, dz \qquad (3)$$

where t is the specimen thickness. The quantitative interpretation of the measured phase shift relies on a number of factors, including (i) the variation in electrostatic potential within the specimen as a function of position along the electron beam direction, (ii) the presence of external fields, (iii) the accurate determination of the local specimen thickness and (iv) the specimen orientation, i.e. the effect of dynamical diffraction on the interaction of the electron wave with the potential. These factors will now be discussed in more detail, in order to explore the experimental procedures that are required to measure electrostatic potentials in semiconductor device structures quantitatively using medium resolution off-axis electron holography.

Two-Dimensional Off-Axis Electron Holography of Semiconductor Devices

Influence of the Specimen Surface

In order to relate the phase shift measured using off-axis electron holography to the electrostatic potential in the specimen, the electrostatic potential distribution as a function of position in the direction of the electron beam must be deduced. Unless only electrostatic fringing fields in vacuum are of interest, a specimen examined using off-axis electron holography must be electron-transparent. Early results suggested that, in order to optimize the signal-to-noise ratio for Si-based devices, the specimen thickness should be in the range of 200–400 nm (Rau *et al.* 1999). A wide range of methods can be used to prepare specimens of this thickness, but only a few of these approaches are used routinely owing to restrictions imposed by the specimen geometry required for off-axis electron holography. These approaches include wedge (tripod) polishing, Ar ion beam milling and FIB milling. The choice of method used for specimen preparation determines the physical and electrical properties of the surfaces of the thin TEM specimen. Surface (Shockley) states are expected to pin the Fermi energy at approximately mid-band gap, which would give rise to a specimen surface layer that is depleted of charge carriers. However, the true nature of the surface potential is usually unknown, and the nature and the thickness of this charge-depleted surface layer cannot be predicted accurately. Early experimental results obtained using off-axis electron holography proposed the use of the concept of electrically "dead" layers to describe near-surface regions that are affected by specimen preparation as shown schematically in Figure 5(a). McCartney *et al.* (2002) used wedge polishing followed by low-angle Ar ion milling to prepare n-MOS and p-MOS Si-based transistors for examination using off-axis electron holography. A wedge-shaped specimen of an Si p–n junction device was also prepared for TEM

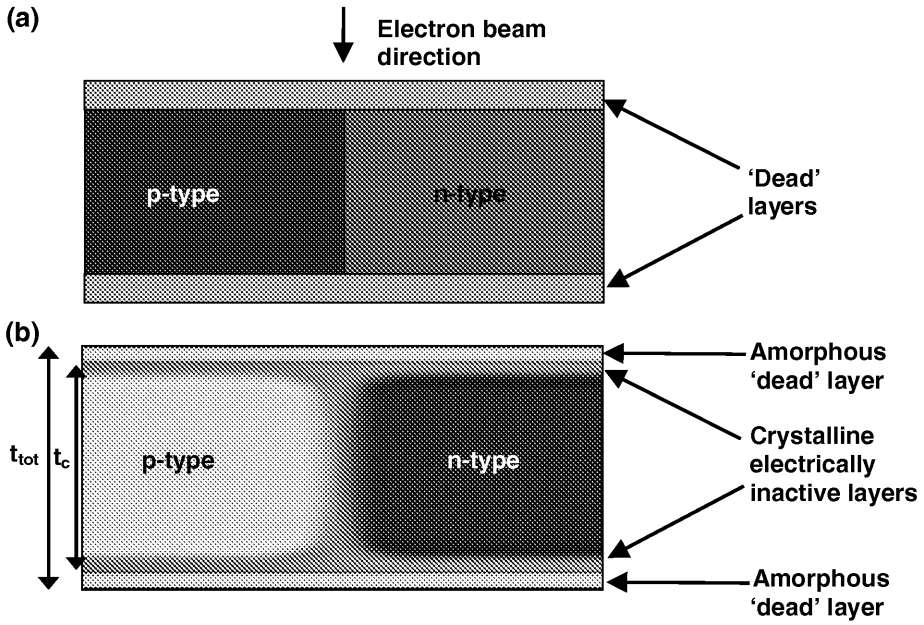

Fig 5. (a) Schematic illustration of a cross-section of a TEM specimen exhibiting electrically "dead" layers at the specimen surfaces. The properties of the p–n junction are assumed to be independent of position along the electron beam direction within the central section (colored blue and red) of the TEM specimen. For simplicity, the thicknesses of the electrically "dead" layers are also assumed to be independent of position along the specimen surface. (b) Schematic diagram illustrating the expected variation in electrostatic potential in a TEM specimen prepared using ion milling. The electrically active properties of the specimen are expected to vary as a function of depth. [The color version of this figure can be seen online at www.interscience.wiley.com/sca.]

examination using the same method. Through examination of the phase change as a function of specimen thickness, the total "dead" layer thickness was determined to be approximately 50 nm. This measurement was then used to interpret results obtained from the transistor structures to obtain two-dimensional quantitative maps of the electrostatic potential distribution. Although the concept of a surface "dead" layer is useful, as it allows surface effects arising from electronic states present on the specimen surface to be taken into account, its use is simplistic, as the charge-depleted surface layer thickness is expected to depend on the local electrically active dopant concentration (Somodi 2006). Therefore, the thickness of the "dead" layer is expected to depend on dopant concentration and species, in addition to being dependent on the specimen preparation method used.

By using the concept of an electrically "dead" layer, the phase shift of the electron beam passing through a semiconductor specimen can be re-expressed according to the equation

$$\phi = C_E V(x,y)(t - 2t_0) \quad (4)$$

where t_0 is the thickness of the electrically "dead" layer on each specimen surface. The surface layers are expected to have a lower electrically active dopant concentration than that in the "bulk-like" central region of the specimen. The observed phase shift is therefore expected to vary more slowly across the junction close to the specimen surfaces than deeper in the TEM specimen. If Poisson's equation is used to calculate the electrically active dopant concentration from the measured projected potential, then the presence of electrically modified surface layers will give rise to an apparently lower electrically active dopant concentration than in the bulk device.

Surprisingly, not all studies of semiconductor devices performed using off-axis electron holography have revealed the presence of "dead" layers at the specimen surfaces. In semiconductor devices prepared using tripod polishing followed by Ar ion milling, McCartney *et al.* (2002) observed electrostatic charge to be present on the specimen surfaces as a result of the interaction of the electron beam with semi-insulating layers within the specimen. A thin layer (30–40 nm) of amorphous carbon deposited on one side of the specimen was used to provide a conduction path to dissipate this charge. Following carbon coating, the expected electrostatic potential distribution was recovered, without needing to take into consideration electrically depleted or "dead" layers on the specimen surfaces.

FIB milling is an alternative specimen preparation method that is now widely used as it allows TEM specimens to be prepared from site-specific areas of devices. However, FIB milling is known to result in the formation of amorphized specimen surface layers, in addition to near-surface layers that have modified electrical properties. The amorphous layers are typically 20–25 nm in thickness on each surface for Si specimens when prepared with a 30 kV Ga beam at glancing incidence to the specimen surface (Giannuzzi and Stevie 2005). A number of studies have been conducted using FIB milling to prepare specimens for examination using off-axis electron holography. However, quantification of the results is complicated by the need to interpret the effect on the potential of Ga ion implantation and damage at the specimen surfaces. Earlier work by Twitchett *et al.* (2002) suggested the presence of 25-nm-thick electrically "dead" crystalline layers close to each specimen surface, in addition to amorphous surface layers. The modified crystalline surface layers may result from the generation of point defects by knock-on damage brought about by the 30 kV Ga ion beam, as well as from doping by the Ga ions. The expected variation in electrostatic potential in an FIB-prepared specimen is shown schematically in cross-section in Figure 5(b). The electrically active dopant concentration varies as a function of depth from the amorphous–crystalline interface in the specimen, increasing to a maximum in the central "bulk-like" region. The presence of the thick near-surface layers gives rise to a minimum specimen thickness before any electrically active material is present in the center of the membrane. Recent results have indicated that a minimum specimen thickness of 350 nm is required before true "bulk-like" properties can be detected in the center of an Si membrane prepared using 30 kV Ga ions (Twitchett-Harrison *et al.* 2007), although this value is expected to depend on dopant concentration. Very recent work has also been used to show how annealing can be used to re-activate dopants in TEM specimens, reducing the thicknesses of electrically dead layers and leading to closer-to-bulk-like variations in electrostatic potential measured across p–n junctions (Cooper *et al.* 2006).

Influence of External Electrostatic Fields

External electrostatic fields arising from charge distributions in TEM specimens can only be measured easily by using phase-sensitive imaging techniques, and are therefore frequently undetected in conventional TEM studies of semiconductor device structures. However, the presence of external electrostatic fields must be considered when quantifying experimental results acquired from semiconductor devices using off-axis electron holography. These

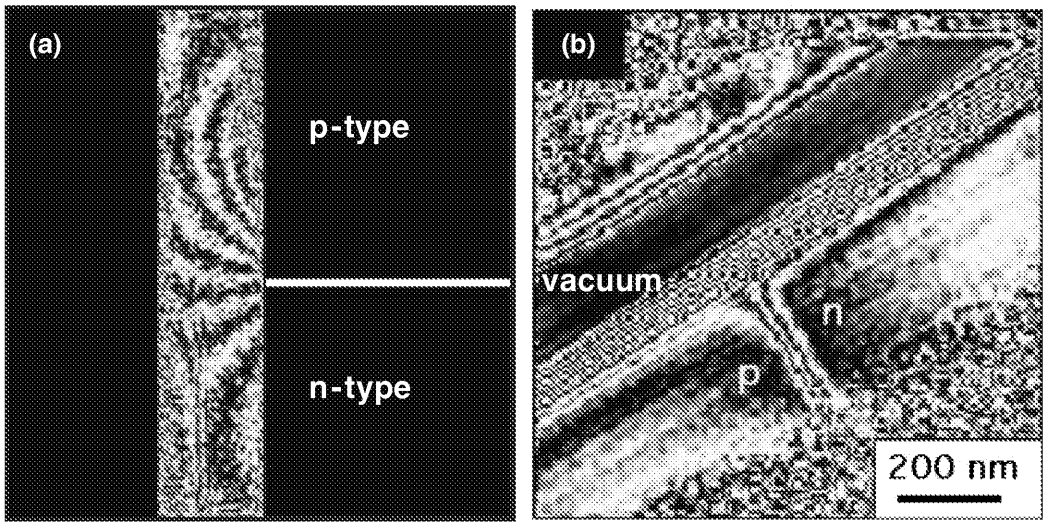

Fig 6. (a) Four-times-amplified phase image showing the electrostatic fringing field outside a 90° Si cleaved wedge containing a p–n junction examined at 2 V applied reverse electrical bias. A zero bias hologram was used as the reference hologram. (b) Four-times-amplified phase image of an FIB-prepared Si p–n junction confirming the absence of external electrostatic fringing fields.

long-range electrostatic fields must be incorporated into two aspects of the interpretation of off-axis electron holography results: first in the phase shift generated as the electron beam passes through the electrostatic field above and below the specimen, and second in the perturbation of the reference wave as a result of the presence of a potential distribution outside the specimen edge. Figure 6(a) shows, in the form of a four-times-amplified phase image, the projected electrostatic potential distribution measured in the vacuum region immediately outside an Si wedge containing a reverse-biased p–n junction. Previous work (Frabboni *et al.* 1987) compared simulations of the three-dimensional electrostatic potential arising from a reverse-biased Si p–n junction with experimental electron holographic data. The simulations highlighted the importance of the lateral separation between the object and reference waves, as well as the comparison of simulated results with experimental data, for the quantitative interpretation of the measured phase shift. In practice, most experimental electron holographic studies involve the use of specimen preparation methods that reduce or remove the expected electrostatic external fields. These methods include using carbon coating or FIB milling to create a conductive surface layer that acts as an equipotential surface and eliminates all external electrostatic fields.

The experimental measurement of external electrostatic fields has only been reported from specimens that were electrically biased in the TEM. Early reports showed that external fields arising from unbiased Si p–n junctions did not produce significant perturbations in reconstructed phase images. However, when the same specimens were examined under reverse electrical bias, external fields were resolved clearly. More recently, electron holography has been used to assess whether external electrostatic potential distributions are present outside FIB-prepared specimens. Figure 6(b) shows a reconstructed phase image acquired from an Si p–n *junction* specimen of uniform thickness prepared using a 30 kV Ga ion beam. Whereas Figure 6(a) showed that a cleaved wedge specimen exhibited an external electrostatic potential distribution similar to that expected (Missiroli *et al.* 1997), the result from the FIB-prepared specimen shown in Figure 6(b) reveals no external electrostatic potential variation, indicating that the specimen surfaces are equipotentials and that only the internal electrostatic potential contribution to the phase shift needs to be considered when interpreting experimental off-axis electron holography results from FIB-prepared specimens. The absence of external electrostatic fringing fields may need to be reassessed for semiconductor devices that have different compositions, or that have been prepared using lower-energy FIB milling, particularly if they are electrically biased.

Influence of Specimen Thickness

Specimen thickness is a key parameter that must be determined accurately to relate phase shifts measured using electron holography to internal electrostatic potential distributions in semiconductor devices. In a TEM specimen, the term "specimen thickness" can refer to two important experimental measurements: the total specimen

thickness, which includes both amorphous and crystalline material, and the crystalline specimen thickness (as illustrated in Figure 5). Energy-filtered TEM is frequently used to obtain maps of total specimen thickness (Egerton 1996), t_{tot}, in units of inelastic mean free path, λ_{tot}. When considering specimens with amorphous surface layers, the projected specimen thickness is a sum of the thicknesses of the constituent layers, and $t_{tot}/\lambda_{tot} \approx (t_a + t_c)/\lambda_{tot}$, where t_a and t_c are the amorphous and crystalline specimen thicknesses, respectively. This expression assumes that λ_{tot} does not vary between the amorphous and crystalline regions of the specimen. In practice, the inelastic mean free path depends on a number of factors (Egerton 1996) including beam convergence, objective aperture size and atomic number, and will be different for the surface of a semiconductor TEM specimen where oxide layers or ion implantation is present (Li *et al.* 2003). t/λ maps can also be measured from reconstructed amplitude images obtained using off-axis electron holography (Gajdardziska-Josifovska *et al.* 1993), although the values of λ are in general different for the two techniques. Convergent beam electron diffraction (CBED) can be used to provide an accurate (± 10 nm) experimental measurement of *crystalline* specimen thickness (Kelly *et al.* 1975). The specimen must be tilted to a zone axis or two-beam condition to be able to determine the specimen thickness, either analytically or through comparisons with simulations of CBED discs. This technique, however, measures the thickness only at the position of the electron beam. If a specimen has varying thickness, then care must be taken to ensure that thickness measurements are taken across the entire area of interest.

Influence of Dynamical Diffraction

When examining crystalline semiconductor devices in the TEM, strong dynamical diffraction will occur if the specimen is oriented close to a zone axis. Away from strongly diffracting orientations, the crystal potential can be approximated by a uniform and constant mean inner potential V_0. Any phase change measured across a junction can then be ascribed to the desired potential change across the depletion region. In the presence of strong dynamical diffraction, the potential can no longer be approximated by V_0 and the measured phase cannot be related directly to the p–n junction potential change. In modern semiconductor device structures, the presence of heterogeneous interfaces can give rise to complex strain fields and local variations in diffraction condition. These strain fields can restrict the orientation of the TEM specimen if a weakly diffracting condition is required, while (usually) maintaining the junction of interest approximately edge-on to the electron beam. For quantitative interpretation of the phase shift, it is essential that the diffraction conditions of the specimen are controlled and unwanted diffraction contrast is minimized.

Three-Dimensional Electron Holography

Electron holography is not restricted to two dimensions, but can be extended to reveal the three-dimensional electrostatic potential distribution within a semiconductor device if combined with electron tomography. Through the acquisition of a tilt series of electron holograms over a wide range of specimen tilt angles, the three-dimensional electrostatic potential within a TEM specimen can be reconstructed using approaches based on back-projection (Twitchett-Harrison *et al.* 2007). The three-dimensional nature of semiconductor device potentials can then be explored experimentally, and the influence on the potential of surface states and surface layers can be visualized directly and separated from the "bulk" potential.

As stated above, phase images modulated by dynamical effects cannot be interpreted easily and should be excluded from any tomographic reconstruction. In the absence of dynamical diffraction, the natural logarithm of the (normalized) holographic amplitude image will be inversely proportional to the cosine of the specimen tilt angle. Images that deviate from this trend suggest the presence of dynamical diffraction, and phase images at these tilt angles should then be excluded from the

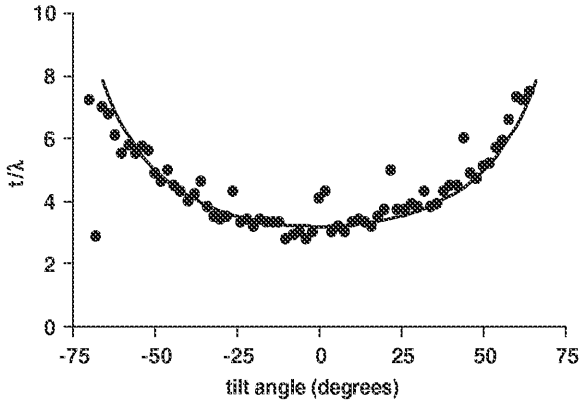

Fig 7. Plot of projected thickness, in units of inelastic mean free path determined from holographic amplitude images, plotted as a function of specimen tilt angle for an FIB-prepared Si p–n junction. Holograms that have been strongly affected by dynamical diffraction are recognized as they lie away from the marked inverse cosine trendline.

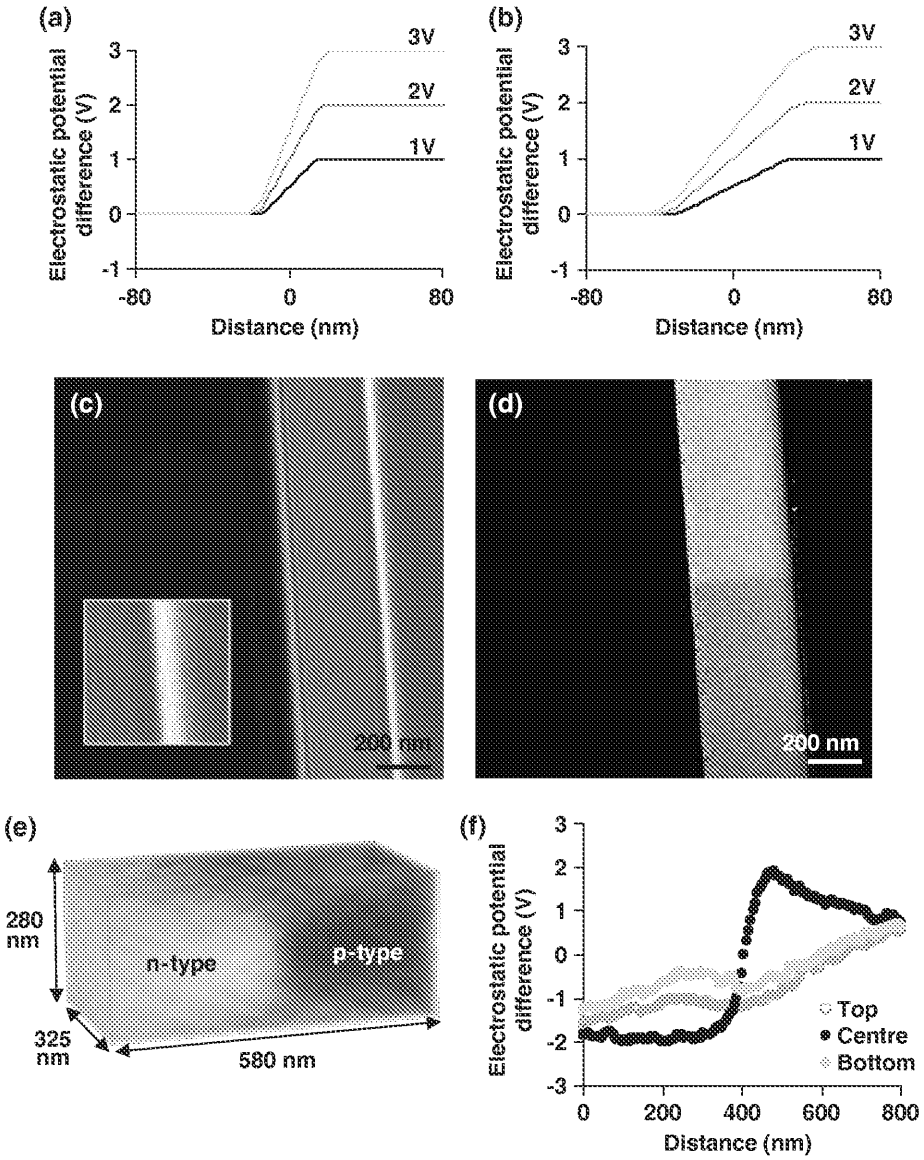

Fig 8. (a) Plot of the theoretical variation in electrostatic potential for a symmetrical abrupt junction with an electrically active dopant concentration of $5 \times 10^{18}\,\mathrm{cm}^{-3}$ as a function of applied reverse bias. The electrostatic potential for an unbiased junction has been subtracted from the total potential, thereby revealing only the potential changes that arise from the application of the electrical bias. (b) Corresponding plot for an electrically active dopant concentration of $1 \times 10^{18}\,\mathrm{cm}^{-3}$. (c) Off-axis electron hologram and (d) corresponding reconstructed phase image of an FIB-prepared Si p–n junction device. The magnified inset in (c) shows the holographic interference fringes. (e) Tomographic reconstruction of the difference electrostatic potential in the FIB-prepared Si device examined at an applied reverse bias of 3 V. The electrically inactive crystalline and amorphous surface layers have been excluded from the reconstruction and are not shown. Substantial modification of the electrostatic potential from that expected in a bulk device can be seen near the top and bottom surfaces of the specimen, and arises from a combination of specimen preparation effects and semiconductor surface depletion layers. (f) Voxel line traces extracted across the p–n junction from the top, center and bottom of the tomographic reconstruction in (e), showing the variation in the electrostatic potential as a function of position along the length of the specimen in a direction perpendicular to the junction. The traces from the top and bottom show a more slowly varying electrostatic potential across the position of the junction than at the center of the membrane, suggesting the presence of a lower electrically active dopant concentration near the surfaces of the specimen.

reconstruction of the three-dimensional electrostatic potential. An example of such a plot, in which deviations from the trendline indicate strong dynamical effects, is shown in Figure 7.

In order to characterize the three-dimensional electrical potential in an FIB-prepared TEM membrane experimentally, "difference" electrostatic potential tomograms were obtained by acquiring experimental tilt series of off-axis electron holograms of an FIB-prepared Si p–n junction specimen with nominal p- and n-type dopant concentrations of $5 \times 10^{18}\,\mathrm{cm}^{-3}$ at 0, 2 and 3 V applied reverse

electrical bias. These holograms were reconstructed to reveal the three-dimensional electrostatic potential for each value of the applied electrical bias. Difference tomograms were obtained by taking the 0 V tomogram as a "reference" to generate tomograms that reveal only changes in electrostatic potential resulting from the application of a reverse electrical bias to the specimen. Ideally, all of the applied voltage should be dropped across the depletion region present at the position of the p–n junction and the width of the depletion region should increase with applied reverse bias. Figure 8(a) and (b) shows the theoretical profiles for the predicted variation in potential across an abrupt symmetrically doped reverse-biased p–n junction, with the electrostatic potential variation for an unbiased junction subtracted to reveal only the contribution to the potential arising from the applied voltage, for electrically active dopant concentrations of (a) $5 \times 10^{18}\,\mathrm{cm}^{-3}$ and (b) $1 \times 10^{18}\,\mathrm{cm}^{-3}$. For the lower electrically active dopant concentration, the applied reverse bias is dropped across a wider depletion region. Figure 8(c) shows an off-axis electron hologram acquired at 0° tilt from an unbiased p–n junction, and Figure 8(d) shows the corresponding reconstructed holographic phase image. Before tomographic reconstruction, phase images such as that shown in Figure 8(d) were adjusted to set the average phase shift across the p and n regions to zero. The tomographic reconstructions therefore reveal only the dopant-related electrostatic potential variation and not the underlying mean inner potential. Figure 8(e) shows the reconstructed difference experimental tomogram for the p–n junction device examined at 3 V reverse bias, using the 0 V tomogram as a "reference." The tomogram thickness was constrained to correspond to the "electrically active" region within the specimen as defined above. The crystalline specimen thickness was measured using CBED to be 330 nm, whereas the tomograms were constrained to be 280 nm in thickness, taking into account the presence of the near-surface crystalline electrically "dead" layers.

Voxel traces taken from the top, center and bottom of the tomographic reconstruction are plotted in Figure 8(f). These profiles reveal that the applied electrical bias is dropped across the electrically active thickness of the specimen, giving rise to an electrostatic potential change of ~3 V across the junction at all positions (top, center and bottom) within the electrically active specimen thickness. However, the slowly varying nature of the change in potential at the top and bottom of the specimen indicates that the electrically active dopant concentrations are much lower than that at the center of the specimen. The depletion width at the center of the specimen is consistent with an electrically active dopant concentration of $\sim 4 \times 10^{17}\,\mathrm{cm}^{-3}$, whereas at the top and bottom of the specimen the electrically active dopant concentration is inferred to be only $\sim 2 \times 10^{17}\,\mathrm{cm}^{-3}$.

The advent of the capability to image electrostatic potentials in three dimensions is of particular interest for current and future device generations, in which three-dimensional nanometer-scale doped regions form the active regions of the device structures. However, further development of the technique is still required in order to reduce the artifacts introduced during the holographic and tomographic reconstruction processes, and to improve the spatial and phase resolutions of the reconstructed three-dimensional data sets. Modern microscopes with ultra-high mechanical and electrical stabilities and high brightness field emission guns offer the chance for considerable improvement in these measurements.

Conclusions

Building on the success of other electrically sensitive SEM and TEM techniques, off-axis electron holography can be used to determine two- and three-dimensional nanometer-scale electrostatic potential distributions in semiconductor device structures. For quantitative interpretation of the measured electron holographic phase shift, a number of factors must be controlled carefully and considered in order to ensure that the correct electrostatic potential distribution is recovered. Specimen preparation, external electrostatic fields, diffraction conditions and variations in specimen thickness must all be considered to ensure that phase shifts measured using off-axis electron holography can be interpreted quantitatively and provide accurate and precise measurements of electrostatic potential distributions in semiconductor devices.

Acknowledgements

The authors are grateful to T. J. V. Yates for contributions to this study and to D. Cooper and P. K. Somodi for discussions. The authors acknowledge financial support from the European Union under the Framework 6 program under a contract for an Integrated Infrastructure Initiative Reference 026019 ESTEEM. Philips Research (Eindhoven) is thanked for providing Si specimens.

References

Cooper D, Twitchett AC, Somodi PK, Midgley PA, Dunin-Borkowski RE, *et al.*: Improvement in electron

holographic phase images of focused-ion-beam-milled GaAs and Si p–n junctions by in situ annealing. *Appl Phys Lett* **88**, 063510 (2006).
Cowley J: Twenty forms of electron holography. *Ultramicroscopy* **41**, 335–348 (1992).
Egerton RF: EELS in the Electron Microscope, Springer, Berlin (1996).
Frabboni S, Matteucci G, Pozzi G: Observation of electrostatic fields by electron holography: the case of reversed biased p–n junctions. *Ultramicroscopy* **23**, 29–38 (1987).
Gabor D: Microscopy by reconstructed wavefronts. *Proc R Soc A* (*Lond*) **197**, 454–487 (1949).
Gabor D: Microscopy by reconstructed wavefronts II. *Proc Phys Soc B* **64**(6), 449–469 (1951).
Gajdardziska-Josifovska M, McCartney MR, de Ruijter WJ, Smith DJ, Weiss JK, *et al.*: Accurate measurements of mean inner potential of crystal wedges using digital electron holograms. *Ultramicroscopy* **50**, 285–299 (1993).
Giannuzzi LA, Stevie FA: Introduction to Focused Ion Beams: Instrumentation, Theory, Techniques and Practice, Springer, Berlin (2005).
Holt DB, Yacobi B: Extended Defects in Semiconductors: Electronic Properties, Device Effects and Structures, Cambridge University Press, Cambridge (2007).
International Technology Roadmap for Semiconductors. (2007). Available at http://www.itrs.net/.
Ishizuka K: Optimized sampling schemes for off-axis holography. *Ultramicroscopy* **52**, 1–5 (1993)
Kelly PM, Jostons A, Blake RG, Napier JG: Determination of foil thickness by scanning transmission electron microscopy. *Phys Status Solidi* (*a*) **31**, 771–780 (1975).
Li J, McCartney MR, Smith DJ: Semiconductor dopant profiling by off-axis electron holography. *Ultramicroscopy* **94**, 149–161 (2003).
Lichte H: Parameters for high resolution electron holography. *Ultramicroscopy* **51**, 15–20 (1993).
McCartney MR, Gribelyuk MA, Li J, Ronsheim P, McMurray JS, *et al.*: Quantitative analysis of one-dimensional dopant profile by electron holography. *Appl Phys Lett* **80**, 3213–3215 (2002).
McMurray JS, Kim J, Williams CC: Quantitative measurement of two-dimensional dopant profile by cross-sectional scanning capacitance microscopy. *J Vac Sci Technol B* **15**, 1011–1014 (1997).
Midgley PA: An introduction to electron holography. *Micron* **32**, 167–184 (2001).
Missiroli GF, Matteucci G, Pozzi G: Electron holography of long-range electrostatic fields. *Adv Imaging Electron Phys* **99**, 171–240 (1997).
Perovic DD, Castell MR, Howie A, Lavoie C, Tiedje T, *et al.*: Field-Emission SEM imaging of compositional and doping layer semiconductor superlattices. *Ultramicroscopy* **58**, 104–113 (1995).
Rau WD, Schwander P, Baumann FH, Höppner W, Ourmazd A: Two-dimensional mapping of the electrostatic potential in transistors by electron holography. *Phys Rev Lett* **82**, 2614–2617 (1999).
Somodi PK: Ph.D. Thesis, University of Cambridge (2006).
Thompson K, Flaitz PL, Ronsheim P, Larson DJ, Kelly TF: Imaging of arsenic Cottrell atmospheres around Si defects by three-dimensional atom probe tomography. *Science* **317**, 1370–1374 (2007).
Tsukamoto K, Yoshikawa S, Toujou F, Morita H: Application of SIMS in microelectronics. *Appl Surf Sci* **203–204**, 404–408 (2003).
Twitchett AC, Dunin-Borkowski RE, Midgley PA: Quantitative electron holography of biased semiconductor devices. *Phys Rev Lett* **88**, 8302–8305 (2002).
Twitchett-Harrison AC, Yates TJV, Newcomb SB, Dunin-Borkowski RE, Midgley PA: High-resolution three-dimensional mapping of semiconductor dopant potentials. *Nano Lett* **7**, 2020–2023 (2007).